Engineered microtissues for the bystander therapy against cancer

Barbara Blanco-Fernandez,[a,†] Irene Cano-Torres,[a,b,†] Cristina Garrido,[a,b,c] Gerard Rubi-Sans,[a,b] Lourdes Sanchez-Cid,[b,c] Marta Guerra-Rebollo,[b,c,d] Nuria Rubio,[b,c] Jeronimo Blanco,[b,c] Soledad Perez-Amodio,[e,a] Miguel A. Mateos-Timoneda[a,f,*] and Elisabeth Engel[e,a,b,*].

[a] Biomaterials for Regenerative Therapies, Institute for Bioengineering of Catalonia (IBEC), The Barcelona Institute of Science and Technology (BIST), 08028, Barcelona, Spain.
[b] Networking Research Center on Bioengineering, Biomaterials and Nanomedicine (CIBER-BBN), 28040, Madrid, Spain.
[c] Cell Therapy Group, Catalonian Institute for Advanced Chemistry (IQAC-CSIC), 08034, Barcelona, Spain.
[d] Grup d'Enginyeria de Materials (Gemat), Institut Químic de Sarrià (IQS), Ramon Llull University (URL), 08017, Barcelona, Spain.
[e] Department of Materials Science and Engineering, EEBE, Technical University of Catalonia (UPC), Barcelona, Spain.
[f] Bioengineering Institute of Technology, Universitat Internacional de Catalunya (UIC), 08195 Sant Cugat del Vallès, Spain.
[*] Corresponding authors: Miguel A. Mateos-Timoneda and Elisabeth Engel, Institute for Bioengineering of Catalonia (IBEC), Carrer de Baldiri Reixac, 10-12, 08028, Barcelona, Spain. e-mails: mamateos@ibecbarcelona.eu ; eengel@ibecbarcelona.eu
[†] These authors are joint first authors and contributed equally to this work.

Keywords: Self-assembled cell-based microtissues, bystander therapy, adipose mesenchymal stem cells, cancer, bioluminescence.

ABSTRACT:

Thymidine kinase expressing human adipose mesenchymal stem cells (TK-hAMSCs) in combination with ganciclovir (GCV) are an effective platform for antitumor bystander therapy in mice models. However, this strategy requires multiple TK-hAMSCs administrations and a substantial number of cells. Therefore, for clinical translation, it is necessary to find a biocompatible scaffold providing TK-hAMSCs retention in the implantation site against their rapid wash-out. We have developed a microtissue (MT) composed by TKhAMSCs and a scaffold made of polylactic acid microparticles and cell-derived extracellular matrix deposited by hAMSCs. The efficacy of these MTs as vehicles for TK-hAMSCs/GCV bystander therapy was evaluated in a rodent model of human prostate cancer. Subcutaneously implanted MTs were integrated in the surrounding tissue, allowing neo-vascularization and maintenance of TK-hAMSCs viability. Furthermore, MTs implanted beside tumors allowed TK-hAMSCs migration towards tumor cells and, after GCV administration, inhibited tumor growth. These results indicate that TK-hAMSCs-MTs are promising cell reservoirs for clinical use of therapeutic MSCs in bystander therapies.

1. Introduction

Cellular therapy, transferring cells into the body to heal/replace impaired cells or tissues, holds promising potential for treating cancer, proved by the numerous ongoing clinical trials [1]. Among the different cell therapy approaches, the use of mesenchymal stem cells (MSCs), as Trojan horses to release anti-cancer molecules in the tumor site, has enormous possibilities [2]. MSCs have shown tropism towards the tumor, having the ability to migrate to the tumor site through chemotaxis [3]. This behavior is explained by the several cytokines and chemokines receptors expressed on the MSCs surface, and the chemotactic proteins secreted by tumor cells [3]. Moreover, MSCs are relatively non-immunogenic, reducing the possibility of immune rejection once transplanted [4]. Its evasiveness privilege enables their use in allogenic conditions, making them suitable candidates for cell therapy [5]. Moreover, MSCs can be easily transduced to induce the production of exogenous proteins [6,7], using adenovirus or lentivirus vectors [8]. Therefore, their tumor tropism and its easy genetically modification features makes them appropriate cellular vehicles for tumor-suppressing therapies [9]. Indeed, they have been bioengineered to produce cytokines [3], growth factor antagonists [10], antiangiogenic factors [11], or prodrug-converting enzymes [12,13]. They have been even loaded with oncolytic virus [14] or anti-cancer drugs [15]. Its efficacy has been shown *in vitro* and *in vivo* for several cancer models [8]. Moreover, there are 14 clinical trials using MSCs for cancer treatment up to date. For instance, there is a bone marrow MSC carrying an oncolytic adenovirus which has proven to be safe and to have anti-tumor effects [16].

One of the approaches followed in cancer treatment uses MSCs is the suicide gene therapy. This approach has also been explored with other mammalian cells showing tumor tropism such as endothelial progenitor cells [17] or T cells [18], amongst others. It consists on the administration of a non-toxic pro-drug that can be converted into a cytotoxic molecule through enzymes expressed by MSCs carrying the suicide gene [19]. One of the most used enzymes for this strategy is thymidine kinase (TK) encoded by herpes simplex virus [19]. TK catalyzes the phosphorylation of deoxythymidine. The broad substrate specificity of TK enables the phosphorylation of a wide diversity of nucleotide analogs, including ganciclovir (GCV) [20]. GCV is a synthetic deoxyguanosine analog used as antiviral drug in cytomegalovirus infection [21]. Its phosphorylation to triphosphate-GCV by TK promotes cell apoptosis by inhibiting the DNA polymerase and the chain termination [20,22]. TK in combination with GCV has been widely explored for the treatment of several types of cancer, relying its efficacy mostly on the bystander effect [23–26]. Its effect consists in the response spreading beyond the transduced cells. Phosphorylated GCV is transferred from dying transduced cells to neighboring non-transduced cells by gap junctions or passive transportation (leading to apoptosis of non-transduced cells). Released phosphorylated GCV and the endocytosis of apoptotic vesicles amplify the drug response. MSCs expressing TK combined with GCV have shown promising results for

the treatment of several types of cancer, such as glioblastoma [27–29], breast cancer [30], melanoma [31], and colon [32], amongst others. Among all MSC types [33], human adipose tissue-derived MSCs (hAMSCs) have similar tumor tropism, surface markers and differentiation capacity as bone marrow-derived MSCs [34–36]; but they are more abundant and easier to extract, and culture than other MSCs types.

Besides, MSCs have also a great potential for the treatment of many other pathologies as neurodegenerative disorders (Parkinson's disease, Alzheimer's disease), renal diseases (acute kidney disease), or myocardial regeneration, amongst others. Indeed, they are currently several clinical trials ongoing for wound healing, Crohn's disease-related fistulas, a phase III study, osteoarthritis, multiple sclerosis, etc [37]. Moreover, they have even show efficacy in the treatment of respiratory failure and the exaggerated cytokine response of the recently discovered COVID-19 disease [38,39][40]. For instance, hAMSC have shown their effectiveness promoting wound healing by differentiating them into epithelial and endothelial cells in animal models or by the production of several paracrine factors. hAMSCs promote the re-epithelialization, angiogenesis and granulation tissue deposition in the wound site.

Previous reports have shown the potential of TK-AMSC/GCV for the treatment of prostate cancer [41] and glioblastoma [29,42]. Vilalta and colleagues showed that this platform could reduce 1.5% prostate cancer cells compared with the control. However, clinical translation has shown limited results, as they will require a substantial number of cells to have a therapeutic effect [41]. After *in vivo* MSCs inoculation, the amount of MSCs rapidly decreases, endangering the efficacy of the therapy as the quantity of therapeutic cells in the tumor area is essential [43–46]. Indeed, the development of new strategies to improve the persistence of the MSCs in the tumor could benefit the clinical usage of this technique, especially in the case of tumor resection [43–45].

Cell-based microtissues (MTs) are a novel approach for bioengineering regenerative therapies and disease modeling [47–51], especially as building blocks for the fabrication of artificial organs [50]. We hypothesize that the use of TK-hAMSCs MTs could be beneficial for having an adequate number of MSCs at the tumor site and, therefore, for achieving a better therapeutic outcome of the TK/GCV platform.

In this work, we evaluate the applicability of TK-hAMSC MTs as vehicles for a bystander therapy consisting in the TK/GCV system. MTs were fabricated using microcarriers (MCs), as they have been successfully used to construct cell MTs [52,53]. Herein, TK-hAMSCs were seeded on top of polylactic acid (PLA) MCs coated with collagen type I. TK-hAMSCs proliferated and deposited different extracellular matrix (ECM) proteins, connecting the MCs and forming a hybrid scaffold consisting of PLA and ECM. These scaffolds are biocompatible, support cell grow and can serve as TK-hAMSCs reservoirs. For studying the *in vivo* efficacy of this platform, a model of prostate cancer was used. TK-hAMSC and tumor cells expressing luciferase reporters were tracked *in vivo* using non-invasive bioluminescence (BLI).

2. Materials and Methods

2.1. Materials

Poly(lactic-acid) (PLA, Purasorb® PLDL 7038) was purchased from Purac®. Human recombinant collagen type I (hrCol1) was obtained from FibroGen (USA). AMD3100, ammonium hydroxide (NH_4OH), bovine serum albumin (BSA), DNAse I, ethyl-(dimethylaminopropyl) carbodiimide (EDC), (-)-Ethyl-L-lactate (photoresist grade; purity>99.0%), formalin, 4-(2-hydroxyethyl)-1-piperazineethanesulfonic acid (HEPES), N-hydroxysuccinimide (NHS), polybrene, polyvinyl alcohol (PVA, 9-10 kDa, 80% hydrolyzed), paraformaldehyde (PFA), polyethylenimine (PEI), poly-D-lysine (PDL), sodium chloride (NaCl), sodium hydroxide (NaOH), sucrose, and triton X-100, were acquired from Sigma-Aldrich. Mouse antibody against RFP (ab65856), Alexa 647 donkey anti-mouse (ab150107), chicken polyclonal antibody anti-GFP (ab13970), goat Alexa 488 anti-chicken (ab150169), rabbit anti-CD31 (ab28364), goat Alexa Fluor 488 anti-rabbit (ab150081), rabbit anti-collagen IV (ab65869), goat anti-rabbit Alexa 488 (ab150081), rabbit anti-collagen I (ab34710) and Platelet Derived Growth Factor-BB (PDGF-BB), were obtained from Abcam. Advanced DMEM, DAPI, fetal bovine serum (FBS), L-glutamine and penicillin/streptomycin were acquired from Thermo-Fisher. The rest of the reagents were acquired from: coelenterazine, PJK-GmbH; D-luciferin subtract, Regis Technologies; fibroblast growth factors (bFGF), Peprotech; ganciclovir (GCV, Cymevene®), Roche; ketamine (Imalgene®), Merial Laboratorios; NanoFuel solvent, Nanolight technology; O.C.T.Tissue-Tek; Opticol™ rat tail collagen I, Cell guidance systems; and xylazine (Rompum®), Bayer.

2.2. Cell lines

hAMSCs were isolated from the adipose tissue of a cosmetic sub-dermal liposuction of an anonymous donor with his consent (Delfos hospital) as previously described [54]. Hek-293T/17 cells (ATCC, CRL-11268) were cultured in DMEM and hAMSCs and human PC3 prostate cancer cells (ATCC, CRL-1435) were cultured in Advanced DMEM, all supplemented with 10% FBS, 2 mM L-glutamine, and 100 units/mL of penicillin and 100 µg/mL of streptomycin. For hAMSCs expansion, cell media was supplemented with 10 ng/mL bFGF.

2.3. Microcarriers fabrication

PLA MCs were prepared by an emulsification/solvent evaporation method, using ethyl-lactate as solvent [55]. Briefly, PLA was dissolved in ethyl-lactate (3.5% w/v) and extruded through a double-bore needle (inner 30G) at a dispensing rate of 10mL/h. A coaxial nitrogen flow was applied (1 atmosphere) for breaking the PLA solution jet into droplets. PLA MCs were precipitated into a hydro-alcoholic bath (0.3 % PVA in

70% v/v ethanol). Particles were left under stirring to harden for 1-2 hours. Then, several washes were done to remove any remaining solvent, using a 40 μm pore sieve (CISA S.A, Spain). The surface of the MCs was then decorated with hrCol1[56]. The hydrolysis of the ester bonds of PLA MCs surfaces using 0.5M NaOH for 60 min was performed. The exposed COOH groups were then activated with a 0.1M EDC/0.2M NHS solution in 70% ethanol for 2h. Afterwards, activated MCs were incubated with a 100 μg/mL rhCol1 solution in PBS overnight. Finally, functionalized MCs were washed and freeze-dried and kept in the fridge until further used. MCs size was measured taking images of the MCs suspension in water using an optical microscope (Leica E600) and FIJI software [57]. To confirm the collagen grafting, MCs were blocked with BSA, incubated with a rabbit antibody against human collagen I, washed and conjugated to Alexa 488 anti-rabbit antibody.

2.4. Lentiviral particles production and cellular transduction

PC3 cells were transduced to express Photinus pyralis luciferase (Pluc) and enhanced green protein (eGFP) [41]. Whereas, hAMSCs were genetically modified to express Renilla reniformis luciferase (Rluc), monomeric red fluorescent protein (mRFP) and a truncated version of herpes simplex virus-TK (tTK), with higher activity than the wild type [29,41,58]. Two lentiviral constructs previously described [41] were used to transduce both cell types, CMV:hRLuc:mRFP:tTK (TK) for hAMSCs and CMV:PLuc:eGFP for PC3 (PG). PG construct consists on an eGFP and PLuc genes under the control of the SV40 and cytomegalovirus promoters, respectively. They were inserted in between the *Cla*I and *Bam*HI sites cassette of Plox/Twgfp lentiviral transfer vector [41]. TK construct is a chimeric trifunctional reporter containing mRFP1, RLuc and tTK (sr39tk) gene controlled by a cytomegalovirus promoter and described elsewhere [58].

Lentiviral constructs were packaged in using the viral envelope plasmid pCMV-VSV-G (Addgene) and the packaging construct pCMV-dR8.2 dvrp (Addgene). Briefly, Hek-293T/17 cells were seeded in a PDL-coated plate adding 25 mM HEPES to the cell media. Next day, cell media was replaced with fresh media containing 25 mM HEPES without FBS or antibiotics.

Each lentiviral construct (6 μg) was mixed with the viral envelope plasmid (pMD-GVSV- G) (2 μg), the packaging plasmid (pCMV DR8.2) (4 μg) and NaCl 150 μM (to have a final volume of 250 μL). A PEI solution (50μL of PEI 0.22 mg/mL with 250 μL of NaCl 150 μM) was added to the DNA solution dropwise and incubated for 30 min at room temperature, to then be added to the Hek-293T/17 cells. After an overnight incubation, the cell media was replaced for fresh media and incubated for another 48h. Afterwards, the supernatant was collected, centrifugated, filtered through 0.45μm and kept at -80ºC until further use.

For cellular transduction, each lentiviral particle suspension was supplemented with polybrene (8 μg/mL) and incubated with the cells for 48h. hAMSC was incubated with TK particles and PC3 with PG ones. Cells were sorted by fluorescence-activated sorting using an Aria^{TM} IIIFACS (BD).

2.5. TK-hAMSCs-MTs production

Cells were seeded into the MCs under dynamic conditions using a spinner flask bioreactor. TK-hAMSCs were seeded on PLA MCs with a cell/MCs ratio of 1×10^6 cells/100mg MCs using a spinner flask bioreactor with a glass ball impeller (Bellco). An intermittent agitation (3min at 30 rpm/27 min 0 rpm) was used for 6h; and then, 1.5mg of colonized MCs were transferred to ultra-low attachment 24-well plates (Corning®). Then, colonized MCs were placed in low attachment plates for several days. MTs are produced after 8 days through the production of ECM, being formed by the combination of ECM, MCs and cells (Fig. 1B). Cell media supplemented with bFGF was changed every 2-3 days. To ensure the cell grafting, 1.5 mg of MCs colonized by cells after the spinner flask seeding were used for a vital staining, using calcein AM/propidium iodide. Cell proliferation was analyzed by BLI. Coelenterazine was solubilized in NanoFuel solvent according to the reagent instructions (3.33 mg/mL) and stored at −80 ºC. For *in vitro* BLI measurements, MTs were washed with PBS and coelenterazine (0.1 mg/mL in PBS) was added. Immediately after its addition, BLI images were recorded using a detection chamber for high-efficiency system provided with an EM-CCD digital camera cooled at −80 ºC (ImagE-MX2, Hamamatsu Photonics). Images were analyzed using the Hokawo 2.6 image analysis software (Hamamatsu Photonics, Deutschland GmbH), and expressed as Photon counts (PHCs) after subtracting the background signal. Arbitrary color bars representing standard light intensity levels were used to generate images.

Surface MTs evaluation was studied with ultra-high resolution filed emission scanning electronic microscopy (SEM, NOVA NanoSEM 230, FEI Company) after 7 days of culture. MTs were fixed with 3% PFA for 10 min at 4 ºC, washed twice with PBS, dehydrated using ethanol gradients, and dried by critical point drying. Afterwards, samples were sputtered with carbon and observed by SEM. To ensure the presence of ECM, MTs were stained against collagen IV after fixing them with paraformaldehyde 4%, permeation with triton X-100 0.1% and blocking with BSA 4% (rabbit anti-Collagen IV/ goat Alexa 488 anti-rabbit).

2.6. In vitro cell migration studies

The effect of tumor-derived conditioned medium on hAMSC migration from the MTs was assessed using a transwell migration assay in a modified Boyden chamber. MTs were used as produced (TK-hAMSCs-MTs) or reseeded with hAMSC after the decellularization (reseeded-TK-hAMSCs-MTs) (SI). TK-hAMSCs-MT and reseeded-TK-hAMSCs- MT were incubated with AMD3100 (20 μg/mL) for 30 min prior to the migration assay. Conditioned medium was recollected from PG-PC3 cultures (SI).

TK-hAMSCs-MTs and reseeded-TK-hAMSCs-MTs with/without previous incubation with AMD3100 were placed in Corning FluoroBlok™ Cell culture inserts (0.8 □m pore size, VWR) and then embedded in 100 μL of Opticol™ rat tail collagen I. After 30 min at 37 □C, collagen polymerized forming a 3D environment for cell migration. Then, they were covered with 100 μL of low-serum medium. Inserts were then placed in the 24-well plates, and the lower chambers were filled with 550 μL of low-serum medium (negative control), PG-PC3-conditioned medium or 100 ng/mL of PDGF-BB (positive control). After 48h, cells at the bottom of the inserts were fixed in 4% PFA. Cell nuclei were stained with DAPI, and the number of migrating cells were counted using a fluorescence inverted microscope.

2.7. Availability of TK-hAMSCs-MTs subcutaneously implanted

TK-hAMSCs-MTs were subcutaneous (SC) implanted on the back of five SCID mice purchased from Charles River (USA) and maintained in a pathogen-free environment. All animal-related procedures were approved by the Government of Catalonia, protocol number 4565. Four MTs per mice were implanted. Animals were anesthetized intraperitoneally with xylazine/ketamine. TK-hAMSCs behavior was tracked by *in vivo* BLI. Images were acquired immediately after the intravenous injection of coelenterazine (150 μL, 0.1 mg/mL) on days 0, 3, 7, 11, 14, 18, 27 and 32. To increase the sensitivity of the signal, the noise signal was reduced by adding together the light events recorded by arrays of 4x4 adjacent pixels (binning 4x4), or exceptionally binning 1×1 (photons at 4x4 can be converted to 1x1 using appropriate scaling factor); and activating the Electron Multiplier (EM) function of the CCD camera. An additional image using white light was obtained to register the location of the signal.

2.8. In vivo treatment of PG-PC3 tumors with TK-hAMSCs-MTs and GCV

Animals were anesthetized as described in section 2.7 and PG-PC3 cells (5×10^5) were subcutaneous (SC) inoculated in the back (anterior position) of SCID mice (n = 12). Six days after cells inoculation, mice were divided in control group - no treatment -, TK-hAMSCs-MTs group - MTs implanted in the proximity of tumors with NaCl 0.9% (SS) administration- and TK-hAMSCs-MT + GCV group - MTs implanted in the proximity of tumors with GCV administration. MTs were implanted next to the tumor (n = 9). On the next day, mice were treated intratumorally with 200 μL of either SS (n = 4, TK-hAMSC-MT) or GCV 10 mg/mL (n = 5, TK-hAMSC-MT + GCV). SS or GCV treatments were repeated daily. PG-PC3 tumor-bearing mice not receiving any treatment (n = 3) were considered as controls. No GCV group was used as without the tTK expression it doesn't have any activity in tumor killing. Tumor progression was weekly monitored by *in vivo* BLI. Briefly, mice were anesthetized as described before and 150 μl of D-luciferin subtract (16.7 mg/mL in PBS) was administered intraperitoneally. After 15 minutes, tumor was visualized as described in

section 2.7. Tumor volume was also measured once tumors were palpable. It was calculated by caliper, by measuring three diameters and calculated with the following equation (Eq. 1) [59]:

$$Tumor\ volume = \frac{\pi}{6} x\ L\ x\ H\ x\ W\ \ L \times H \times W\ (Eq.\ 1)$$

Being L the length, H the height and W the width.

2.9. Histological analysis

MTs harvested from mice (section 2.7 and 2.8) were washed with NaCl 0.9%, fixed with formalin for 24 hours, treated with sucrose solutions (10%, 20% and 30%), embedded in O.C.T. and sliced in 10 μm sections. RFP$^+$ and GFP$^+$ cells were detected through immunofluorescence, using mouse monoclonal antibody against RFP (1:500)/Alexa-Fluor 647 donkey anti-mouse (1:1000) and chicken polyclonal antibody anti-GFP (1:500)/goat Alexa 488 anti-chicken (1:1000), respectively. Nuclei were counterstained with DAPI (0.2 mg/mL). For immunofluorescence of endothelial cells, cells were labelled using rabbit anti-CD31 (1:500 dilution) and secondary goat anti-rabbit antibody, conjugated with Alexa Fluor 488 (1:1000). Also, 5 μm-sliced samples were stained with hematoxylin-eosin (H/E) according to manufacturer's protocol.

2.10. Statistical analysis

GraphPad Prism 5 Software was used for the statistical analysis of BLI data. When data could be adjusted to a normal distribution the T-test was applied for 2 group comparisons, one-way ANOVA for more than two groups, and two-way ANOVA to compare more than two treatment groups at different times.

3. Results

3.1. PLA MCs enable the cell attachment

PLA MCs were fabricated by a solution jet-break up followed by a solvent displacement method as previously reported by our group [55], which enable the production of highly porous and spherical particles. MCs were fabricated with ethyl lactate, a green-solvent that minimizes the environmental impact and is safe for human health [60]. MC´s surface was covalently functionalized [56] with collagen type I to promote cell attachment. Microscope image analysis showed an average diameter of 55.1 ± 14.4 μm after collagen decoration (Fig. 1A-B). The collagen grafting success was confirmed by immunofluorescence (Fig. 1C). Life/dead staining was performed to ensure that cells were able to attach to the MCs and maintain their viability. Non-transduced hAMSCs were seeded on top of the MCs in dynamic conditions using a spinner

flask during 6h, and then stained with calcein AM/propidium iodide. Cells were able to attach to the carrier's surface maintaining their viability (Fig. 1D).
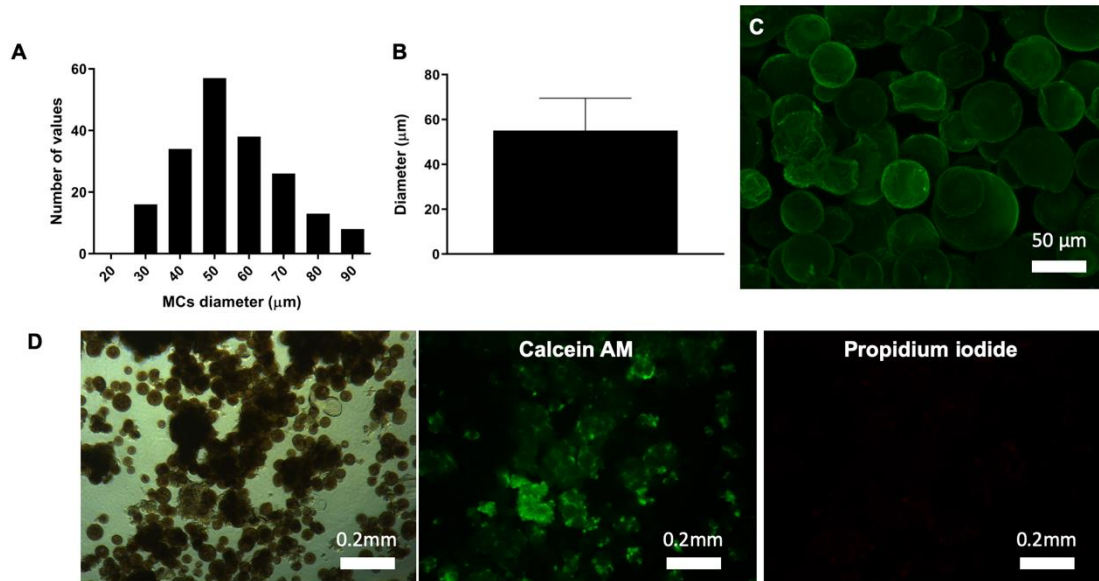

Fig. 1. MCs characterization. (A) Histogram of the distribution size of collagen I decorated MCs. (B) Diameter of the MCs. (C) Immunofluorescence images of the MCs stained with an antibody against collagen type I (green). (D) hAMSC attachment into the MCs and its cell viability staining. From left to right optical image, calcein AM (green) staining and propidium iodide (red) staining of the MCs after seeding them with hAMSCs.

3.2. Photoprotein and fluorescent protein expression by hAMSCs and PC3

hAMSCs cells were successfully transduced with a lentiviral particle obtaining cytotoxic, fluorescent (mRFP) and luminescent (RLuc) genetically modified cells (tTK) for a non-invasive tracking (Fig. 2A). The use of this construct for hAMSCs transduction has shown no effect in cell proliferation or phenotype [29]. On the other hand, PC3 cells were transduced with a gene encoding for green fluorescence (eGFP) and luminescence (PLuc) (Fig. 2A). This approach enables the cell sorting of transduced cells by flow cytometry through RFP+ (hAMSC) or GFP+ (PC3). Moreover, fluorescence marker´s expression also allows the *ex vivo* cell tracking by confocal imaging.

3.3. TK-hAMSCs forms viable MTs and a bio-hybrid scaffold

Formation of MTs was observed between 5 and 6 days of culturing. After 8 days, MCs were completely connected to each other by the ECM secreted by TK-hAMCs, forming a bio-hybrid scaffold of ECM and

PLA MCs (Fig. 2B). These MTs had a relatively malleable shape that would facilitate their inclusion in different tissues. Cultures were extended for up to 18 days to assess proliferation of TK-hAMSCs.
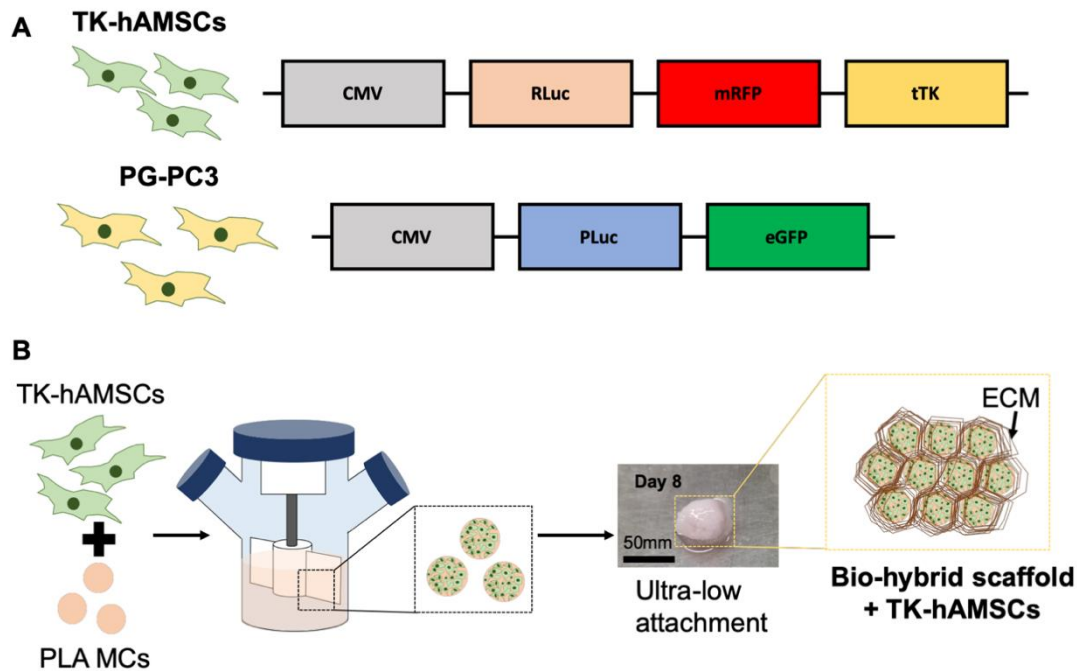

Fig. 2. Schemes of the hAMSCs and PC3 transduction and MTs fabrication. (A) Schematic representation of the encoding genes transduced to PC and hAMSCs. (B) Schematic representation for TK-hAMSCs MTs fabrication.

TK-hAMSCs MTs were also evaluated using SEM after 1 week of culture. SEM shows that MTs reached sizes of 5.5 mm long and 2 mm wide (Fig. 3A). At higher magnifications, it could be observed that cells have a spread morphology (Fig. 3A). Although the presence of the MCs was still evident, they were completely coated by secreted ECM. Also, cross-sectional images showed dense ECM deposition inside the constructs.

To confirm the presence of ECM deposition, a collagen IV immunofluorescence was carried out (Fig. 3B). A high collagen IV deposition was observed around the particles (black holes in the images).

Cellular proliferation in the MTs was measured by BLI. BLI signal emitted by Renilla luciferase expressing TK-hAMSCs is quantitatively correlated with the number of cells through the corresponding calibration curve (Fig. 3C). This allows the monitorization of cellular proliferation in a non-invasive manner. An increase in proliferation was observed up to 7 days (Fig. 3D) Then, the cell number was maintained stable up to 18 days. Changes in cell numbers were not observed from that time point till the end of the culture period
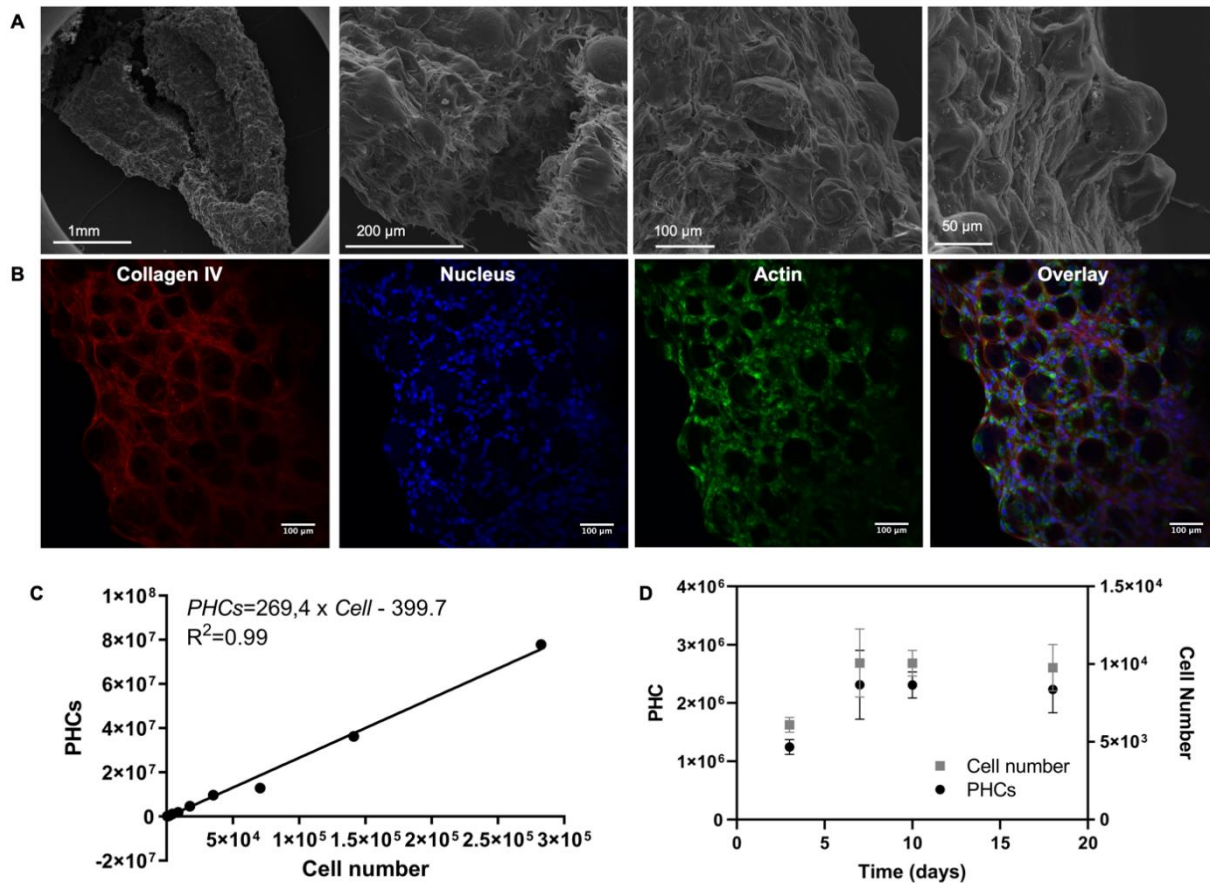
Fig. 3. MTs characterization. (A) SEM images of the TK-hAMSCs MTs after 1 week of culture. A clear ECM deposition can be observed around the MCs. (B) Collagen IV deposition and cell morphology in the TK-hAMSCs MTs. Collagen IV is stained by immunofluorescence (red), nuclei is stained by DAPI (blue) and cytoskeleton is stained by Phalloidin (green). (C) Calibration curve of PHCs emitted by TK-hAMSCs depending on cell number. (D) Cellular proliferation of TK-hAMSCs in the MTs.

3.4. Tumor cells do not promote the in vitro TK-hAMSCs migration from the MTs

hAMSCs migration capacity from MTs towards a tumor chemotactic stimulus was assessed *in vitro* through a transwell migration assay (Fig. 4A). TK-hAMSCs were able to migrate towards the conditioned media (not statistically significant) but in a lower proportion than the positive control (PDGF-bb). We hypothesized that the low migration might be promoted by the cell entrapment in the matrix, hindering cell migration. Thus, we evaluated if recently seeded cells in the scaffold, that should be less adhered to the MT surface, could migrate towards prostate cancer stimulation. MTs were chemically and biologically

decellularized, removing all the cells whereas maintaining the integrity of the proteinaceous ECM (Fig. 4B). TK-hAMSCs were successfully seeded and grown inside the scaffold (Fig. 4C). Howbeit, hAMSCs migration capacity was not enhanced when the MTs were decellularized and reseeded again. MTs were also preconditioned with a CXCR4 antagonist, AMD3100. This compound blocks CXCR4/SDF-1α pathway, which modulates the cell homing effect observed in MSCs niches [61]. Even with the higher numbers of migrating cells, there was no effect of the conditioned media on both, the MTs and reseeded MTs conditions (Fig. 4A).
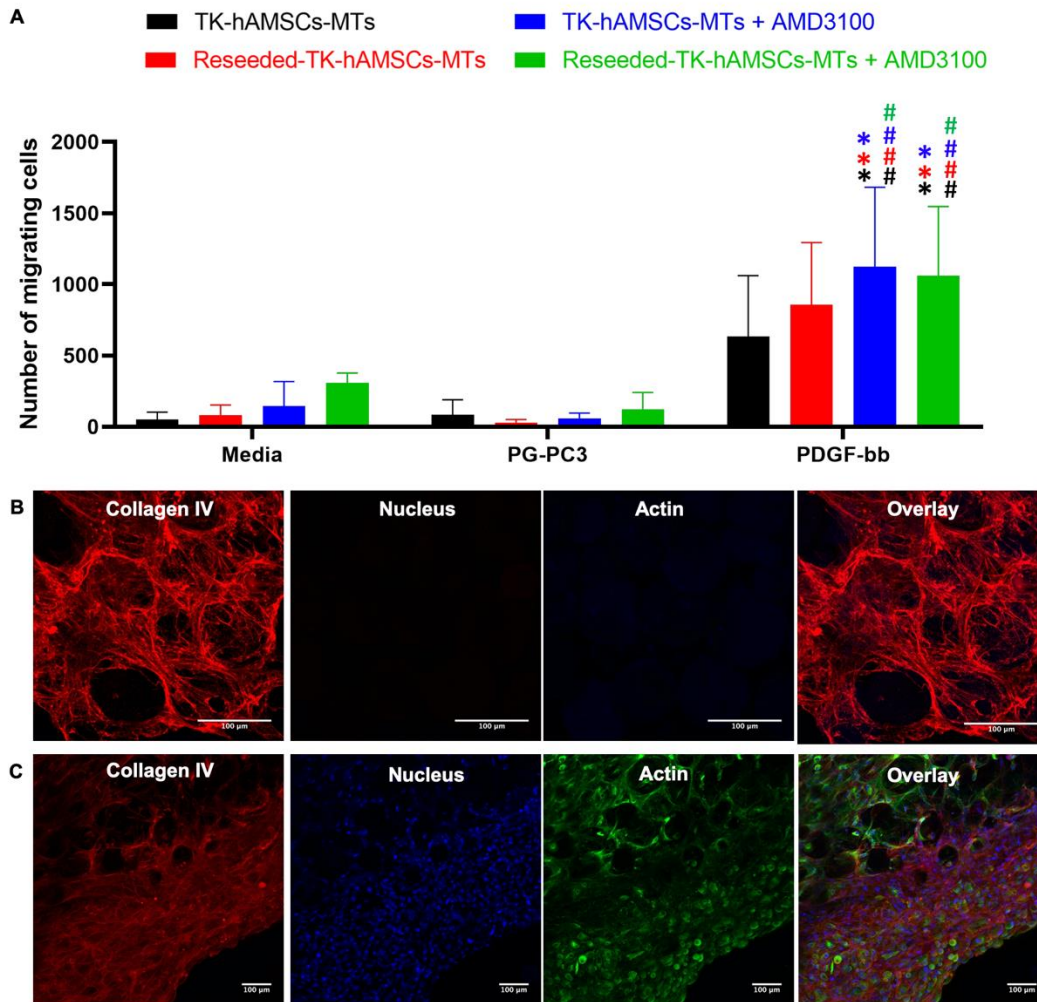

Fig. 4. Transwell migration assay assessing therapeutic TK-hAMSCs mobility from MTs towards PG-PC3 conditioned medium. (A) Quantification of cell migration towards medium with low serum content (medium, negative control), conditioned medium (PG-PC3) and a positive control (PDGF-bb). MTs were used as they were (TK-hAMSC-MT, black), decellularized and reseeded with fresh hAMSCs (reseeded-TK-hAMSC-MT, red), incubated with AMD3100 (TK-hAMSC-MT + AMD3100, blue) or decellularized,

reseeded with fresh hAMSCs and incubated with AMD3100 (reseeded-TK-hAMSC-MT + AMD3100, green). Conditioned medium was not able to stimulate the migration of TK-hAMSCs from MTs. (p≤0.01, Two-way ANOVA, n=3; symbols: * significant vs. media and # vs. PG-PC3). (B-C) Confocal image of MTs after decellularization (B) and after reseeding (C). Collagen IV is stained by immunofluorescence (red), nuclei is stained by DAPI (blue) and cytoskeleton is stained by Phalloidin (green). The decellularization process removed all the cells from the scaffolds and it was possible to reseed them, being mostly located in the outer layer of the scaffold (scale bar, 100 μm).

3.5. TK-hAMSCs-MTs are available up to 32 days after in vivo subcutaneous implantation

TK-hAMSCs-MTs were subcutaneously implanted in the back of five SCID mice (four TK-hAMSCs-MTs per mice) to test the availability of TK-hAMSCs *in vivo*. TK-hAMSCs survival was monitored by *in vivo* RLuc-BLI. During the three first days, a strong cell wash-out was detected, reducing the number of cells. Afterwards, TK-hAMSCs slightly proliferated until day 10 post-implantation. The amount of TK-hAMSCs decreased from day 10th being detectable at least until day 32nd (Fig. 5A and 5B; Fig. S1).
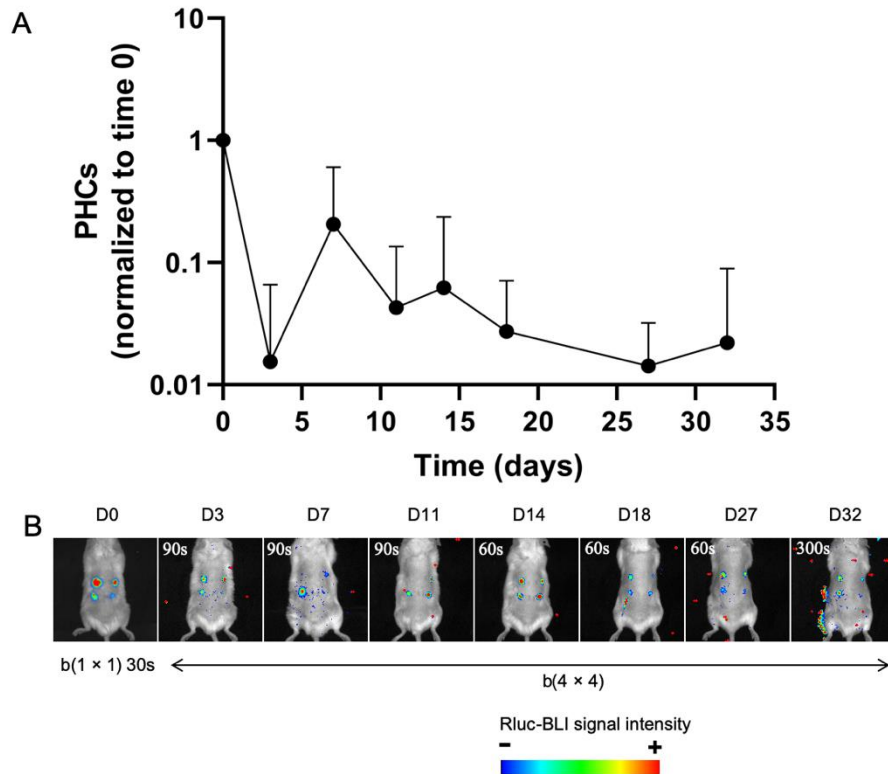

Fig. 5. TK-hAMSCs availability over time by BLI. (A) Changes in light production by TL-hAMSCs after the administration of the MTs. (B) Composite pseudo-color BLI images at different days post MTs

administration (see supplementary data, Fig. S1, for the whole set). The color bar represents the light intensity of RLuc hAMSCs from blue/black low signal to red high signal. PLuc images are superimposed on a black/white image of the same mice.

3.6. TK-hAMSCs-MTs plus GCV inhibit PG-PC3 tumor progression through a bystander effect

To test the antitumor capacity of TK-hAMSCs-MTs/GCV bystander treatment, PG-PC3 were subcutaneously inoculated into SCID mice. After six days, mice were divided into 3 groups: negative control (no treatment), TK-hAMSCs-MTs (MTs implanted in the proximity of PG-PC3 tumors without GCV administration) and TK-hAMSCs-MTs + GCV (MTs implanted in the proximity of PG-PC3 tumors with GCV administration). No differences in bioluminescence were observed at this timepoint between animals. A schematic representation of MTs implantation procedure is shown in Fig. 6A Tumor progression was weekly monitored by *in vivo* BLI due to the small size of the tumors, caliper measurements were recorded after 27 days of tumor inoculation. TK-hAMSCs-MTs/GCV bystander treatment inhibits tumor progression obtaining lower BLI values (2.6-fold) and a smaller tumor volume (4-fold) than control groups (Fig. 6B-D, Fig. 2S). TK-hAMSCs-MTs plus intratumorally administration of SS did not affect tumor progression compared with the control group. Fig. 6D showing harvested MTs and tumors at day 46 indicate that tumors did not engulf MTs.
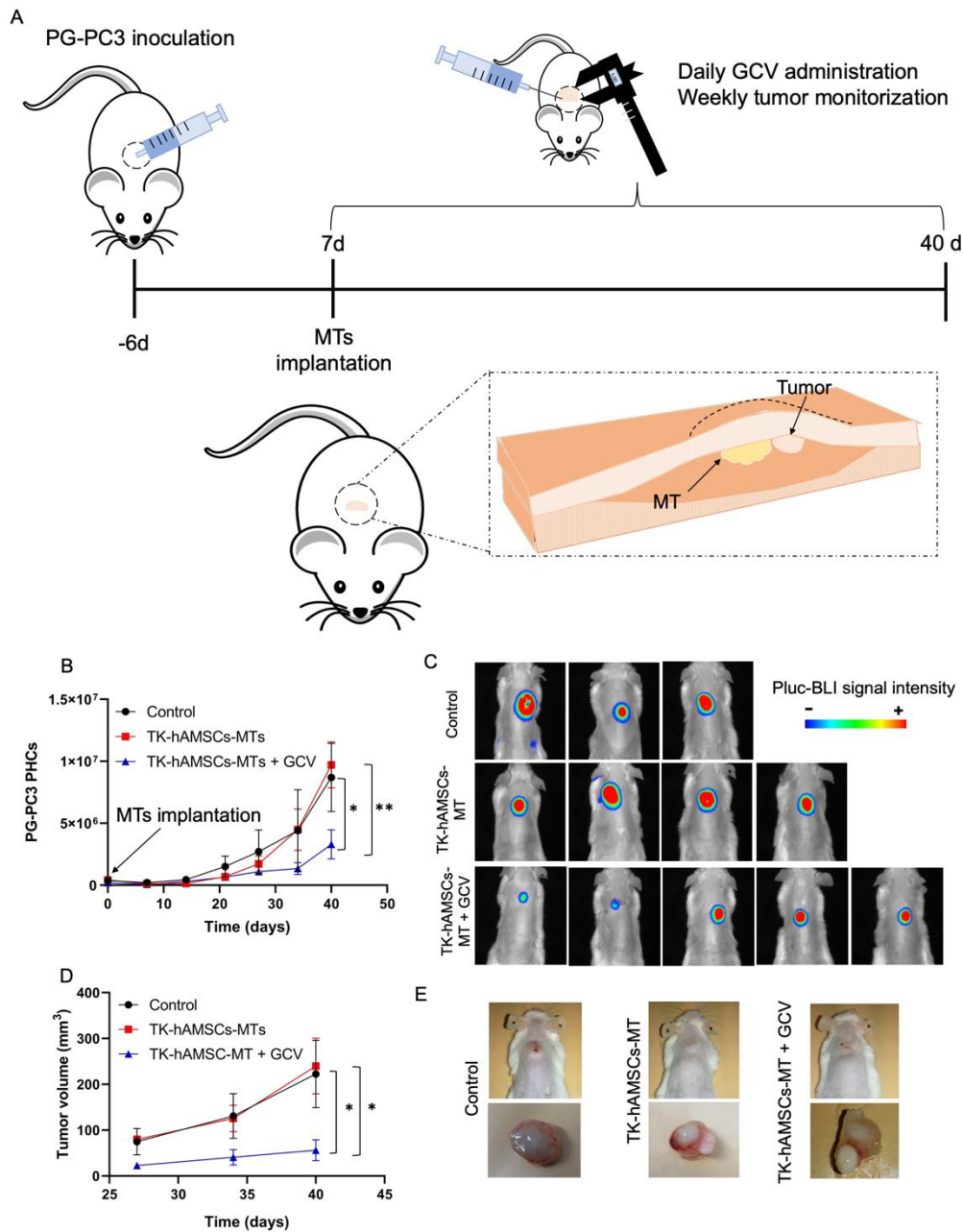
Fig. 6. *In vivo* GCV effect through bystander killing of PG-PC3 by TK-hAMSCs-MTs. PG-PC3 tumor bearing mice were non-treated (control, n=3), treated with TK-hAMSCs-MT and SS (TK-hAMSCs-MT, n=4) or TK-hAMSCs-MT and GCV (TK-hAMSCs-MT + GCV, n=5). (A) Scheme of the time schedule of the bystanther therapy and MT inoculation. (B)Tumor growth by BLI. Changes in the light production by PG-PC3 tumors after the administration of TK-hAMSCs-MTs. (C) Composite pseudo-color BLI images at 46 days post tumor inoculation (see supplementary data, Fig. S2, for the whole set). The color bar represents

the light intensity of PLuc PG-PC3 from blue/black low signal to red high signal. PLuc images are superimposed on a black/white image of the same mice. (D) Tumor volume over time. (E) Tumor images before and after the harvesting from mice at day 46 after of tumor inoculation. Data are presented as the mean ± SEM. (* $p < 0.01$, ** $p < 0.001$, 2-ways ANOVA).

3.7. TK-hAMSCs-MTs allow TK-hAMSCs migration in vivo

PG-PC3 tumors and TK-hAMSCs-MTs were harvested after 46 days of tumor implantation to detect the effective migration of therapeutic cells into the tumor using immunofluorescence. Fig. 7 shows confocal images of the limits between TK-hAMSCs-MTs and non-tumor tissue (Fig. 7B), or with PG-PC3 tumor (Fig. 7C and D). TK-hAMSCs were capable to migrate from MTs to the tumor tissue, being detectable outside the limits of the MT interacting with PC-3 cells (Fig. 7D). Mice treated with MTs without GCV also shown cell migration towards the tumor (Fig. 7A).
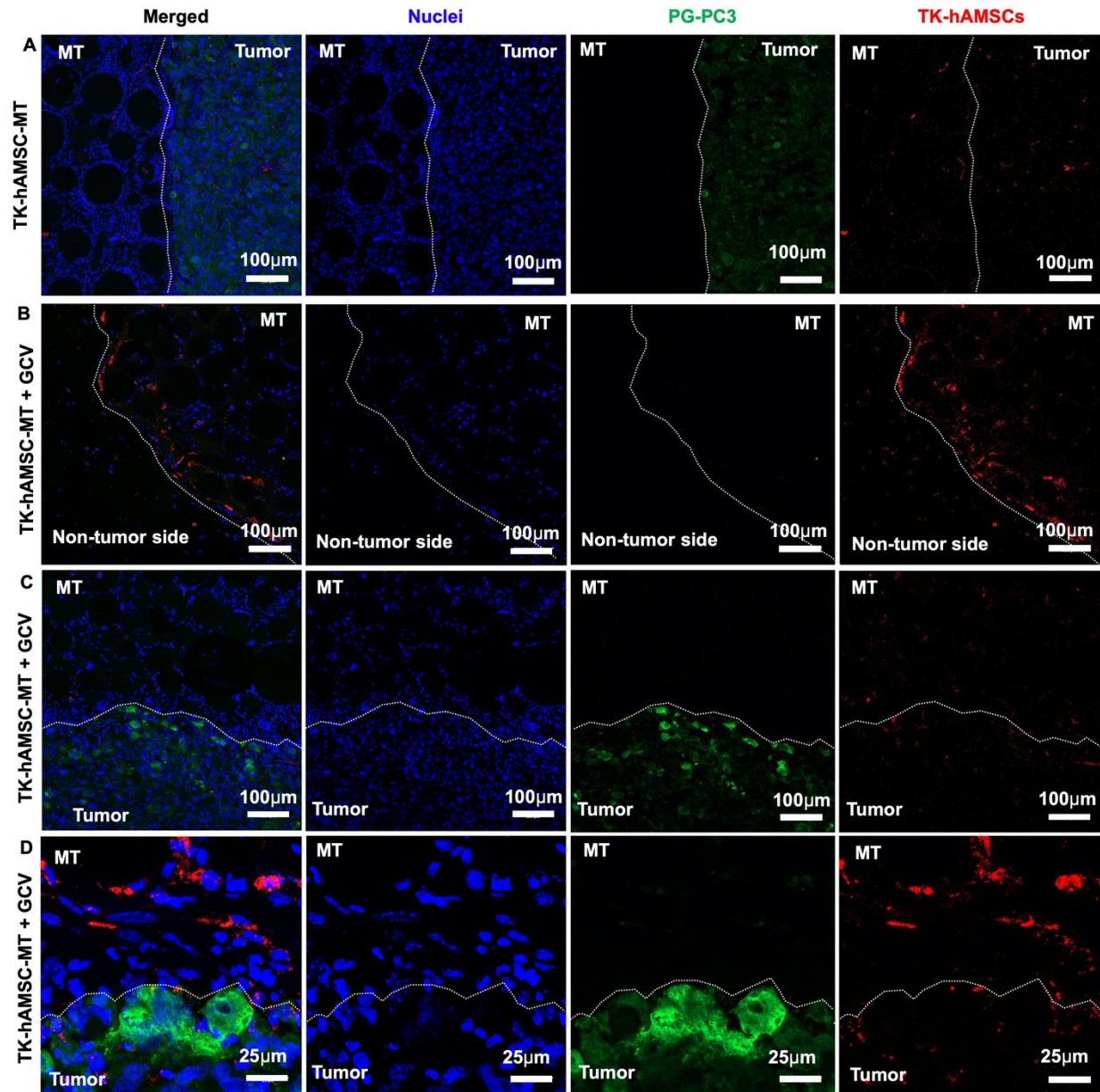
Fig. 7. TK-hAMSCs migration from TK-hAMSCs-MTs towards tumor cells after 40 days of MTs inoculation and 46 days of tumor formation. (A) TK-hAMSCs-MTs/PG-PC3 tumor limits treated with SS. (B) TK-hAMSCs-MTs/non-tumor side limits treated with GCV. (C,D) TK-hAMSCs-MTs/PG-PC3 tumor limits treated with GCV at a lower (C) and higher magnification (D). First row all channels merged, second row nuclei stained with DAPI, third row PG-PC3 cells stained with antibody anti-GFP/Alexa 488 and last row TK-hAMSCs stained with an antibody against RFP/Alexa 647.

3.8. TK-hAMSCs-MTs were irrigated by blood vessels

Harvested PG-PC3/MTs were strongly integrated into the subdermal surrounding tissue and blood vessels were visible on the surface of the MTs. H/E staining showed extensive vascularization inside of the TK-hAMSCs-MTs for both GCV and SS treated conditions (Fig. 8B and C). Eosin intrinsic affinity to erythrocytes exhibited bright red spots throughout the construct, even 1 mm inside the MT, corresponding to vascular lumens. On the contrary, PGPC3 tumors exhibited a high cellular density with blood vessels only discretely presented in peripheric areas (Fig. 8A), indicating hypoxic environments that characterize prostate tumors [62]. To confirm the presence of blood vessels in the MTs, a CD31 immunofluorescence staining was performed. CD31 positive cells were observed inside the MTs, conforming lumen structures (Fig. 8D).
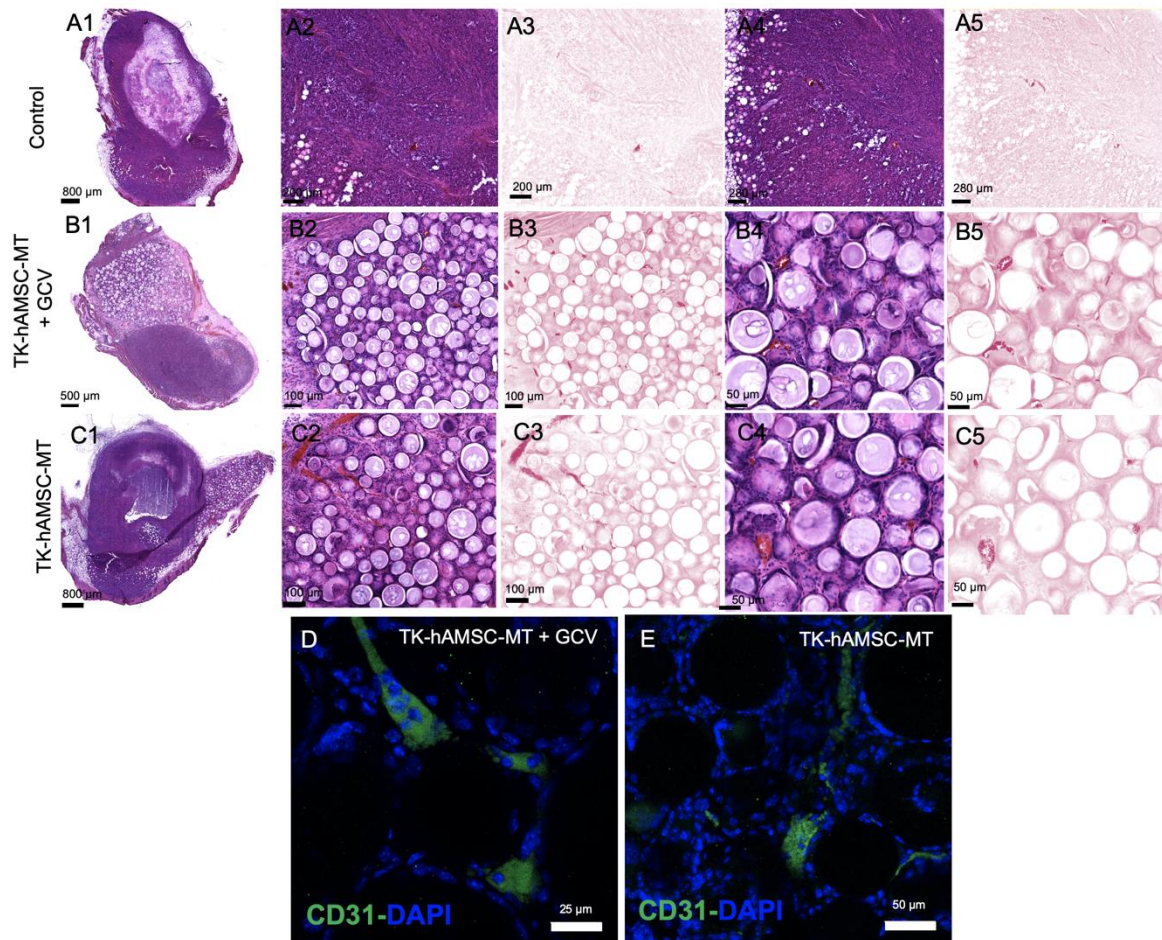

Fig. 8. Vascularization of TK-hAMSCs-MTs. (A-C) Hematoxylin-eosin histological staining of PG-PC3 tumor (A) and TK-hAMSCs-MT/PG-PC3 treated with GCV (B) or non-treated (C) harvested after 40 days of implantation. Eosin enhanced staining of erythrocytes allows the visualization of ingrowth vessels inside

the microtissues (arrowheads). (D, E) Immunofluorescence of blood vessels in the MTs with GCV (D) or saline administration (E). In green, CD31$^+$ cells and in blue nuclei stained with DAPI. CD31$^+$ cells were observed inside the MTs conforming a tubular lumen structure.

4. Discussion

tTK/GCV is one of the most used suicide genes therapy in cancer, either by transducing them in the tumor cells or delivered by a transduced vehicle cell (suicide cells). After the death of the vehicle cell by GCV, neighboring tumor cells uptake the released products and provoke their death by the bystander effect [23–26]. Among all vehicle cell types used for cell therapy, MSCs are a powerful tool for cancer cell therapy [2,3,6–8,10–13] due to its tropism towards the tumor [3] and its immuno-evasiveness [5]. However, MSCs number in the tumor rapidly decrease reducing its efficacy and require multiple applications [43–45]. Although most of the studies have used bone marrow MSCs expressing TK [30–32], hAMSCs have similar tumor tropism but they are easier to obtain and culture [34–36]. Moreover, they have also evidenced their potential for tTK/GCV suicide gene therapy [29,41,42].

Herein, we have developed a bio-hybrid scaffold to increase the persistence of the hAMSCs expressing tTK in the tumor, working as a cell reservoir. Cells are actively contributing to the formation of the bio-scaffold by proliferating and depositing ECM, creating a therapeutic MTs. MCs have already shown their potential for the construction of MTs for tissue engineering [63–67] or even fabricating *in vitro* tumors [68]. Whereas cell-derived ECM scaffolds have been used in different tissue regeneration approaches for bone, cartilage, liver, skin and vascular tissue among others [69]. MTs were prepared through a dynamic seeding of TK-hAMSCs in the PLA MCs, followed by a static incubation over a period of 8 days. The use of this approach enabled MCs colonization by hAMSCs (Fig. 1). Furthermore, PLA MCs connected to the ECM secreted by TK-hAMSCs, forming all together the MTs (Fig. 2B and 3A-B). The scaffold was biocompatible enabling cell proliferation in 3D until day 7 (Fig. 3D). Then, a stationary phase in cell growth was observed. We hypothesize that hAMSCs' proliferation was stopped due to the lack of space in the MT structure [70]. Nevertheless, ECM deposition was strongly induced and did not stop as a consequence of the arrest in cell proliferation (data not shown). The scaffold composition and structure, made of microparticles, acts as a biomimetic cell reservoir supporting cell growth and ECM deposition. These properties will not only provide with new therapeutic cells but can also protect the cells from death.

We hypothesize that hAMSCs MTs could be appropriate vehicles for a bystander therapy consisting in TK/GCV, enabling appropriate numbers of MSCs in the tumor site. These MTs may be useful for clinical applications to *in situ* killing tumor cells at the tumor or rejection site. Indeed, few authors have reported the use of scaffolds encapsulating therapeutic cells for the treatment of glioblastoma [43–45,71]. Sheet and colleagues found out that the encapsulation of tumoricidal neural stem cells into gelatin hydrogels increased

cell persistence in the surgical cavity following tumor resection up to 8 weeks (compared with 3 days for free cells or 8 days for PLA nanofibers) and were permissive to tumor-tropism [43].

In order to test weather our platform can be used as a scaffold to sustain the bioavailability of tumoricidal hAMSCs at the tumor site, we used a tumor model of human prostate cancer (PC3). We decided to use this tumor model due to its easiness and the positive *in vitro* and *in vivo* results previously reported with these tumoricidal cells and tumor [41]. Moreover, currently prostate cancer therapy, which generally relies on prostatectomy and radiotherapy, can lead to erectly dysfunction and urinary incontinency [72]. This platform could ensure the prostate function avoiding prostatectomy or radiotherapy, and their associated side effects.

Vilalta and co-workers proved *in vitro* that GCV was able to kill all TK-hAMSCs after 7 days of treatment. Moreover, when TK-hAMSCs were cocultured with untransduced PC3, 90% killing of PC3 was detected after 7 days treatment with GCV. However, without the addition of GCV, no cell death could be detected. *In vivo*, TK-hAMSCs/GCV platform was efficient killing PG-PC3 tumors when a cell ratio of 1:4 (tumor to hAMSCS) was used. Mice bearing PC3 tumors treated with TK-hAMSCs and GCV induced bystander killing reducing tumor cells to 1.5 % vs control tumors. However, they require a substantial cell number and successive cell inosculations [41]. Herein, we used the same constructs to transduce hAMSCs and PC3, and track the MTs efficacy by *in vivo* BLI.

The ability of hAMSC to migrate towards the tumor cells is highly relevant for the success of the bystander therapy [73]. Herein, we tested the migration capabilities of hAMSC using a transwell model. The MTs were placed into the transwell, and embedded in a collagen hydrogel to guarantee a 3D migration environment. *In vitro* experiments showed a low migratory capacity for TK-hAMSCs in MTs towards PG-PC3 conditioned media. Several factors might be responsible for the observed phenomena. A possible explanation is the high number of integrins binding sites in the MT [74] vs. the low concentration of chemoattractants in the conditioned PG-PC3 derived medium. Another explanation could be the dense ECM deposition in the MTs, which could hinder the cell migration. To ensure that the dense ECM on the MTs was not responsible for the low migration capacity of hAMSCs, MTs were decellularized and reseeded with TK-hAMSCs cells. This approach will ensure that cells are more readily available on the MTs surface, being readily available for migrating towards tumor-secreted chemokines. Decellularized MTs maintained the integrity of the bio-hybrid scaffolds. Cell-free MTs were reseeded with more cells, which were more available on the surface of MTs than its core. However, TK-hAMSCs did not migrate towards the tumor conditioned media. This result suggests that cell entrapment in the dense matrix may not be related to the observed low cell migration.

As CXCR4/SDF-1α axis blocking has also showed enhancement of MSCs migration, we assessed if AMD3100 could enhance the TK-hAMSCs migratory profile. AMD3100 is an CXCR4/SDF-1α axis

antagonist that has showed an enhancement of stem cell mobilization from stem cell niches towards other tissues [75]. Jiang and colleagues showed that AMD3100 increase cell migration towards hypoxic tumors by forcing CXCR4 overexpression, thus sensitizing hAMSCs towards SDF-1α-expressing hypoxic cells [76]. Nevertheless, the use of AMD3100 did not promote cell migration *in vitro* in the MTs.

As PDFG-bb (positive control) was able to stimulate the cell migration in all cases, being no statistical differences between samples, we believe that MTs are not altering the hAMSCs characteristics neither impeding their physical migrations. Therefore, only PG-PC3 conditioned media did not stimulate cell migration *in vitro* at the tested conditions. As mention before, the high number of integrins binding sites in the MT and the chemoattractants concentration in the PG-PC3 derived medium could be the reason for the observed phenomenon. Moreover, MTs were embedded in a collagen hydrogel to guarantee a 3D environment, which might slow down hAMSC migration. For instance, Hesse and colleagues detected MSCs migration only after 7 days in culture in collagen hydrogels [77]. Indeed, we believe that the *in vitro* conditions tested might not be appropriated for testing hAMSC migration, and therefore, a more physiological relevant model could be more suitable to study the cell migration. Thus, we moved forwards with the *in vivo* experiments for testing the migration capabilities of hAMSCs.

The use of BLI demonstrated the survival of therapeutic cells in MTs after, at least, 32 days of implantation. However, a reduction in the signal was observed in the first days, which has also been observed previously after the direct inoculation of hAMSCs [41]. Moreover, in previous studies including scaffolds for retaining stem cells in resected tumor areas have also shown a reduction in the MSC number, being detected only until day 10-28 post-inoculation [43–45]. We hypothesize that the decrease in cell numbers was due to the restricted availability of nutrients and oxygen arriving through diffusion. Indeed, the vascular network growing towards the inner space of microtissues (Fig. 8) could explain the increased in BLI signal observed at day 7 post implantation.

To assess the antitumor potential of the TK-hAMSCs-MTs/GCV bystander platform, a prostate cancer model was used. PG-PC3 cells were subcutaneously injected into immuno-depressed mice to form the tumor model. As PC3 is a hormone-independent tumor [78], a prostate orthotopic implantation was discarded. Moreover, the subcutaneous administration of tumor cells facilitates MT implantation and process standardization, which is necessary to validate this platform [41]. The implanted PG-PC3 cells were left for 6 days to enable the tumor formation. Vilalta and co-workers showed that the number of PG-PC3 injected directly correlate with the bioluminescence signal, even though they were not vascularized [41]. After 6 days, animals were randomly distributed in 3 groups: negative control (no treatment), a MT control (MTs administration without GCV treatment) and treatment group (MTs with GCV treatment). TK-hAMSCs-MTs/GCV bystander treatment significantly inhibited the tumor progression, as shown by the tumor volumes and the BLI results (Fig. 6 and Fig. S2). As particular concerns were aroused by the use of

hAMSCs in bystander therapies due to the effect of MSCs in the progression of some tumors [79,80], we studied whether TK-hAMSCs-MTs had any effect in tumor growth. We could not observe any difference in tumor growth among the control and the MTs, suggesting that hAMSCs did not affect tumor progression. The tTK/GCV platform requires several therapeutic cell administrations to replenish the cells and sustain the therapeutic effect [41]. Interestingly, the use of MTs enable one unique hAMSCs administration. MTs worked as TK-hAMSCs reservoirs, retaining cells in the tumor proximity as well as maintaining their viability.

All animals were sacrificed 40 days after MTs implantation (46 days after tumor inoculation) to study hAMSCs migration towards the tumor. We decided to use this time point to ensure the viability of the hAMSCs in the MTs to test their migratory capacity using immunofluorescence. In addition, controls group (control and TK-hAMSCs-MTs) required euthanasia due to the large volume of tumors at this point. PG-PC3 tumors/TK-hAMSCs-MTs were harvested after 46 days of tumor implantation showing blood vessels at their surfaces. Harvested MTs maintained their integrity and were not engulfed by the tumor in any condition. CD31 and hematoxylin and eosin staining's proved the presence of blood vessels inside the MTs. The neo-vascularization of TK-hAMSCs-MTs not only facilitates the nutrients and oxygen supply for higher TK-hAMSCs survivals *in vivo* over time but also enables the arrival of chemotactic molecules from the tumor.

Therapeutic cell migration was observed from MT regardless the treatment (GCV and SS), demonstrating PG-PC3 potential chemokine attraction on hAMSCs. These *in vivo* results clearly indicated hAMSC tropism towards tumor cells. This might explain the observed TK-hAMSCs migration toward the tumor tissue for an efficient tumor killing effect. However, the bystander effect of TK-hAMSCs located in the tumor limits cannot be discarded, as it might also be responsible of the cancer cell killing death in some extent.

The use of MCs/cell-derived MTs offers a modular approach for the obtaining of any MT shape and size, with soft consistency that allows the inclusion of TK-hAMSCs-MTs in different organs adapting to the structure of the tissue. This property could be beneficial for the implantation in tumor resection cavities to remove any residual tumor cell. Many other tumor models or silencing genes (cytosine deaminase/5-fluorocytosinde) could be benefited from this platform. Moreover, the use of BLI enable tracking the platform efficacy in a non-invasive manner.

5. Conclusions

In this work, we demonstrated that hAMSCs MTs are suitable tTK/GCV platforms for cancer based on bystander killing effect. This platform was tested against a model of prostate cancer, showing promising

results with a unique cell administration dose. Previous studies indicated the requirement of substantial proportion of therapeutic cells and several cell administrations for the effectiveness of the treatment [41]. However, the biohybrid scaffolds made of polymeric materials (PLA MCs) and cell-derived ECM are a suitable reservoir of hAMSCs, requiring only one-time implantation. Factors secreted by the tumor might have contributed to the rapid MT vascularization, aiding in the survival of therapeutic cells. Moreover, hAMSCs showed cell migration towards the tumor in the *in vivo* model GCV/MTs bystander therapy achieved tumor regression against ectopic prostate tumor successfully as well as prolonged hAMSCs retention. This strategy was combined with BLI monitoring demonstrating feasibility of this non-invasive imaging technique to track therapeutic cell survival together with tumor cell fate.

Conflicts of interest

The authors declare no conflicts of interest.

Acknowledgements

References

[1]   J.X. Yu, V.M. Hubbard-Lucey, J. Tang, The global pipeline of cell therapies for cancer, Nat. Rev. Drug Discov. 18 (2019) 821–822.

[2]   A. Nowakowski, K. Drela, J. Rozycka, M. Janowski, B. Lukomska, Engineered Mesenchymal Stem Cells as an Anti-Cancer Trojan Horse, Stem Cells Dev. 25 (2016) 1513–1531.

[3]   M. Mosallaei, M. Simonian, N. Ehtesham, M.R. Karimzadeh, N. Vatandoost, B. Negahdari, R. Salehi, Genetically engineered mesenchymal stem cells: targeted delivery of immunomodulatory agents for tumor eradication, Cancer Gene Ther. (2020). https://doi.org/10.1038/s41417-020-0179-6.

[4]   K. Le Blanc, C. Tammik, K. Rosendahl, E. Zetterberg, O. Ringdén, HLA expression and immunologic propertiesof differentiated and undifferentiated mesenchymal stem cells, Exp. Hematol. 31 (2003) 890–896.

[5]   J.A. Ankrum, J.F. Ong, J.M. Karp, Mesenchymal stem cells: immune evasive, not immune privileged, Nat. Biotechnol. 32 (2014) 252–260.

[6]   C. De Wolf, M. Van De Bovenkamp, M. Hoefnagel, Regulatory perspective on in vitro potency assays for human mesenchymal stromal cells used in immunotherapy, Cytotherapy. 19 (2017) 784–797.

[7]   J. Jiang, D. Wei, L. Sun, Y. Wang, X. Wu, Y. Li, Z. Fang, H. Shang, Z. Wei, A preliminary study on the construction of double suicide gene delivery vectors by mesenchymal stem cells and the in vitro inhibitory effects on SKOV3 cells, Oncol Rep. 31: (2014) 781–787.

[8]   A. Mohr, R. Zwacka, The future of mesenchymal stem cell-based therapeutic approaches for cancer – From cells to ghosts, Cancer Lett. 414 (2018) 239–249.

[9]   K. Shah, Mesenchymal Stem Cells engineered for Cancer Therapy, Adv. .Drug Deliv Rev. 64 (2012) 739–748.

[10]   L. Yang, Y. Zhang, L. Cheng, D. Yue, J. Ma, D. Zhao, X. Hou, R. Xiang, P. Cheng, Mesenchymal Stem Cells Engineered to Secrete Pigment Epithelium-Derived Factor Inhibit Tumor Metastasis and the Formation of Malignant Ascites in a Murine Colorectal Peritoneal Carcinomatosis Model, Hum. Gene Ther. 27 (2016) 267–277.

[11]   Y. Chu, H. Liu, G. Lou, Q. Zhang, C. Wu, Human placenta mesenchymal stem cells expressing exogenous kringle1-5 protein by fiber-modified adenovirus suppress angiogenesis, Cancer Gene Ther. 21 (2014) 200–208.

[12]   I.T. Cavarretta, V. Altanerova, M. Matuskova, L. Kucerova, Z. Culig, C. Altaner, Adipose Tissue-derived Mesenchymal Stem Cells Expressing Prodrug-converting Enzyme Inhibit Human Prostate Tumor Growth, Mol. Ther. 18 (2010) 223–231.

[13]   D.-Y. Chang, S.-W. Yoo, Y. Hong, S. Kim, S.J. Kim, S.-H. Yoon, K.-G. Cho, S.H. Paek, Y.-D. Lee, S.-S. et al Kim, The growth of brain tumors can be suppressed by multiple transplantation of mesenchymal stem cells expressing cytosine deaminase, Int. J. Cancer. 127 (2010) 1975–1983.

[14] A. Hadrys, A. Sochanik, G. McFadden, J. Jazowiecka-Rakus, Mesenchymal stem cells as carriers for systemic delivery of oncolytic viruses, Eur. J. Pharmacol. 874 (2020) 172991.

[15] S. Cheng, S.K. Nethi, S. Rathi, B. Layek, S. Prabha, Engineered Mesenchymal Stem Cells for Targeting Solid Tumors: Therapeutic Potential beyond Regenerative Therapy, J. Pharmacol. Exp. Ther. 370 (2019) 231–241.

[16] A. Hmadcha, A. Martin-Montalvo, B.R. Gauthier, B. Soria, V. Capilla-Gonzalez, Therapeutic Potential of Mesenchymal Stem Cells for Cancer Therapy, Front. Bioeng. Biotechnol. 8 (2020) 1–13. https://doi.org/10.3389/fbioe.2020.00043.

[17] A. Laurenzana, F. Margheri, A. Chillà, A. Biagioni, G. Margheri, L. Calorini, G. Fibbi, M. Del Rosso, Endothelial Progenitor Cells as Shuttle of Anticancer Agents, Hum. Gene Ther. 27 (2016) 784–791. https://doi.org/10.1089/hum.2016.066.

[18] S. Sun, H. Hao, G. Yang, Y. Zhang, Y. Fu, Immunotherapy with CAR-modified T cells: Toxicities and overcoming strategies, J. Immunol. Res. 2018 (2018). https://doi.org/10.1155/2018/2386187.

[19] P. Zarogoulidis, K. Darwiche, A. Sakkas, L. Yarmus, H. Huang, Q. Li, L. Freitag, K. Zarogoulidis, M. Malecki, Suicide Gene Therapy for Cancer – Current Strategies, J Genet Syndr Gene Ther. 4 (2013) 16849.

[20] F. Moolten, Tumor chemosensitivity conferred by inserted herpes thymidine kinase genes: paradigm for a prospective cancer control strategy, Cancer Res. 46 (1986) :5276-5281.

[21] C.S. Crumpacker, Ganciclovir, N. Engl. J. Med. 335 (1996) 721–729.

[22] U. Fischer, S. Steffens, S. Frank, N.G. Rainov, K. Schulze-Osthoff, C.M. Kramm, Mechanisms of thymidine kinase/ganciclovir and cytosine deaminase/ 5-fluorocytosine suicide gene therapy-induced cell death in glioma cells, Oncogene. 24 (2005) 1231–1243.

[23] C. Gu, S. Li, T. Tokuyama, N. Yokota, H. Namba, Therapeutic effect of genetically engineered mesenchymal stem cells in rat experimental leptomeningeal glioma model, Cancer Lett. 291 (2010) 256–262.

[24] S. Kalimuthu, L. Zhu, J.M. Oh, H.W. Lee, P. Gangadaran, R.L. Rajendran, S.H. Baek, Y.H. Jeon, S.Y. Jeong, S.-W. Lee, J. Lee, B.-C. Ah, Regulated Mesenchymal Stem Cells Mediated Colon Cancer Therapy Assessed by Reporter Gene Based Optical Imaging, Int. J. Mol. Sci. 19 (2018) 1002.

[25] C. Leten, J. Trekker, T. Struys, T. Dresselaers, R. Gijsbers, G. Vande Velde, I. Lambrichts, A. Van Der Linden, C.M. Verfaillie, U. Himmelreich, Assessment of bystander killing-mediated therapy of malignant brain tumors using a multimodal imaging approach, Stem Cell Res. Ther. 6 (2015) 163.

[26] F.S. Nouri, X. Wang, A. Hatefi, Genetically engineered theranostic mesenchymal stem cells for

the evaluation of the anticancer efficacy of enzyme/prodrug systems, J. Control Rel. 200 (2015) 179–187.

[27]   X.Y. Bak, D.H. Lam, J. Yang, K. Ye, E.L.X. Wei, S.K. Lim, S. Wang, Human embryonic stem cell-derived mesenchymal stem cells as cellular delivery vehicles for prodrug gene therapy of glioblastoma, Hum. Gene Ther. 22 (2011) 1365–1377.

[28]   S.M. De Melo, S. Bittencourt, E.G. Ferrazoli, C.S. Da Silva, F.F. Da Cunha, F.H. Da Silva, R.S. Stilhano, P.M.A. Denapoli, B.F. Zanetti, P.K.M. Martin, L.M. Silva, A.A. Dos Santos, L.S. Baptista, B.M. Longo, S.W. Han, The anti-tumor effects of adipose tissue mesenchymal stem cell transduced with HSV-Tk gene on U-87-Driven brain tumor, PLoS One. 10 (2015) 1–13.

[29]   M. Alieva, J.R. Bagó, E. Aguilar, C. Soler-Botija, O.F. Vila, J. Molet, S.S. Gambhir, N. Rubio, J. Blanco, Glioblastoma therapy with cytotoxic mesenchymal stromal cells optimized by bioluminescence imaging of tumor and therapeutic cell response, PLoS One. 7 (2012) 1–11.

[30]   L. Leng, Y. Wang, N. He, D. Wang, Q. Zhao, G. Feng, W. Su, Y. Xu, Z. Han, D. Kong, Z. Cheng, R. Xiang, Z. Li, Molecular imaging for assessment of mesenchymal stem cells mediated breast cancer therapy, Biomaterials. 35 (2014) 5162–5170.

[31]   T.Y. Zhang, B. Huang, H. Bin Wu, J.H. Wu, L.M. Li, Y.X. Li, Y.L. Hu, M. Han, Y.Q. Shen, Y. Tabata, J.Q. Gao, Synergistic effects of co-administration of suicide gene expressing mesenchymal stem cells and prodrug-encapsulated liposome on aggressive lung melanoma metastases in mice, J. Control. Release. 209 (2015) 260–271.

[32]   J. Yang, K. Lv, J. Sun, J. Guan, Anti-tumor effects of engineered mesenchymal stem cells in colon cancer model, Cancer Manag. Res. 11 (2019) 8443–8450.

[33]   R. Hass, C. Kasper, S. Bohm, R. Jacobs, Different populations and sources of human mesenchymal stem cells (MSC): a comparison of adult and neonatal tissue-derived MSC, Cell Commun. Signal. 9 (2011) 12.

[34]   K. Nakamura, Y. Ito, Y. Kawano, K. Kurozumi, M. Kobune, H. Tsuda, A. Bizen, O. Honmou, Y. Niitsu, H. Hamada, Antitumor effect of genetically engineered mesenchymal stem cells in a rat glioma model, Gene Ther. 11 (2004) 1155–1164.

[35]   S. Kern, H. Eichler, J. Stoeve, H. Kluter, K. Bieback, Comparative analysis of mesenchymal stem cells from bone marrow, umbilical cord blood, or adipose tissue, Stem Cells. 24 (2006) 1294–1301.

[36]   L. Kucerova, V. Altanerova, M. Matuskova, S. Tyciakova, C. Altaner, Adipose tissue-derived human mesenchymal stem cells mediated prodrug cancer gene therapy, Cancer Res. 67 (2007) 6304–6313.

[37]   L. Shukla, Y. Yuan, R. Shayan, D.W. Greening, T. Karnezis, Fat Therapeutics: The Clinical

Capacity of Adipose-Derived Stem Cells and Exosomes for Human Disease and Tissue Regeneration, Front. Pharmacol. 11 (2020) 1–23. https://doi.org/10.3389/fphar.2020.00158.

[38]   F. Sánchez-Guijo, M. García-Arranz, M. López-Parra, P. Monedero, C. Mata-Martínez, A. Santos, V. Sagredo, J.M. Álvarez-Avello, J.E. Guerrero, C. Pérez-Calvo, M.V. Sánchez-Hernández, J.L. Del-Pozo, E.J. Andreu, M.E. Fernández-Santos, B. Soria-Juan, L.M. Hernández-Blasco, E. Andreu, J.M. Sempere, A.G. Zapata, J.M. Moraleda, B. Soria, F. Fernández-Avilés, D. García-Olmo, F. Prósper, Adipose-derived mesenchymal stromal cells for the treatment of patients with severe SARS-CoV-2 pneumonia requiring mechanical ventilation. A proof of concept study, EClinicalMedicine. 25 (2020). https://doi.org/10.1016/j.eclinm.2020.100454.

[39]   P. Gentile, A. Sterodimas, Adipose-derived stromal stem cells (ASCs) as a new regenerative immediate therapy combating coronavirus (COVID-19)-induced pneumonia, Expert Opin. Biol. Ther. 20 (2020) 711–716. https://doi.org/10.1080/14712598.2020.1761322.

[40]   P. Gentile, A. Sterodimas, Adipose stem cells (ASCs) and stromal vascular fraction (SVF) as a potential therapy in combating (COVID-19)-disease, Aging Dis. 11 (2020) 465–469. https://doi.org/10.14336/AD.2020.0422.

[41]   M. Vilalta, I.R. Dégano, J. Bagó, E. Aguilar, S.S. Gambhir, N. Rubio, J. Blanco, Human adipose tissue-derived mesenchymal stromal cells as vehicles for tumor bystander effect: A model based on bioluminescence imaging, Gene Ther. 16 (2009) 547–557.

[42]   O. Meca-Cortés, M. Guerra-Rebollo, C. Garrido, S. Borrós, N. Rubio, J. Blanco, CRISPR/Cas9-Mediated Knockin Application in Cell Therapy: A Non-viral Procedure for Bystander Treatment of Glioma in Mice, Mol. Ther. - Nucleic Acids. 8 (2017) 395–403.

[43]   K.T. Sheets, M.G. Ewend, M. Mohiti-Asli, S.A. Tuin, E.G. Loboa, K.S. Aboody, S.D. Hingtgen, Developing Implantable Scaffolds to Enhance Neural Stem Cell Therapy for Post-Operative Glioblastoma, Mol. Ther. 28 (2020) 1056–1067.

[44]   J.R. Bagó, G.J. Pegna, O. Okolie, S.D. Hingtgen, Fibrin matrices enhance the transplant and efficacy of cytotoxic stem cell therapy for post-surgical cancer, Biomaterials. 84 (2016) 42–53.

[45]   J.R. Bagó, G.J. Pegna, O. Okolie, M. Mohiti-Asli, E.G. Loboa, S.D. Hingtgen, Electrospun nanofibrous scaffolds increase the efficacy of stem cell-mediated therapy of surgically resected glioblastoma, Biomaterials. 90 (2016) 116–125.

[46]   G. Rubi-Sans, O. Castaño, I. Cano, M.A. Mateos-Timoneda, S. Perez-Amodio, E. Engel, Engineering Cell-Derived Matrices: From 3D Models to Advanced Personalized Therapies, Adv. Funct. Mater. 2000496 (2020) 1–19.

[47]   H. Yin, Y. Wang, X. Sun, G. Cui, Z. Sun, P. Chen, Y. Xu, X. Yuan, H. Meng, W. Xu, A. Wang, Q. Guo, S. Lu, J. Peng, Functional tissue-engineered microtissue derived from cartilage

extracellular matrix for articular cartilage regeneration, Acta Biomater. 77 (2018) 127-141.

[48]   V. Bunpetch, Z.-Y. Zhang, X. Zhang, S. Han, P. Zongyou, H. Wu, O. Hong-Wei, Strategies for MSC expansion and MSC-based microtissue for bone regeneration, Biomaterials. 196 (2019) 67–79.

[49]   D. (Danielle) Huang, S.B. Gibeley, C. Xu, Y. Xiao, O. Celik, H.N. Ginsberg, K.W. Leong, Engineering Liver Microtissues for Disease Modeling and Regenerative Medicine, Adv. Funct. Mater. (2020) 1909553.

[50]   G.H. Lee, J.S. Lee, X. Wang, S.H. Lee, Bottom-Up Engineering of Well-Defined 3D Microtissues Using Microplatforms and Biomedical Applications, Adv Heal. Mater. 5 (2016) 56–74.

[51]   K.-H. Nam, A.S.T. Smith, S. Lone, S. Kwon, D.-H. Kim, Biomimetic 3D Tissue Models for Advanced High-Throughput Drug Screening, J. Lab. Autom. 20 (2015) 201–215.

[52]   C. Palmiero, G. Imparato, F. Urciuolo, P. Netti, Engineered dermal equivalent tissue in vitro by assembly of microtissue precursors, Acta Biomater. 6 (2010) 2548–2553.

[53]   L. Huang, A.M.E. Abdalla, L. Xiao, G. Yang, Biopolymer-based microcarriers for three-dimensional cell culture and engineered tissue formation, Int. J. Mol. Sci. 21 (2020).

[54]   M. Vilalta, I. Degano, J. Bago, D. Gould, M. Santos, M. Garcia-Arranz, R. Ayats, C. Fuster, Y. Chernajovsky, D. Garcia-Olmo, N. Rubio, J. Blanco, Biodistribution, Long-term Survival, and Safety of Human Adipose Non-invasive, Tissue-derived Mesenchymal Stem Cells Transplanted in Nude Mice by High Sensitivity Bioluminescence Imaging, Stem Cells Dev. 17 (2008) 993–1004.

[55]   R. Levato, M.A. Mateos-Timoneda, J.A. Planell, Preparation of biodegradable polylactide microparticles via a biocompatible procedure, Macromol Biosci. 12 (2012) 557–566.

[56]   X. Punet, R. Mauchauffé, M.I. Giannotti, J.C. Rodríguez-Cabello, F. Sanz, E. Engel, M.A. Mateos-Timoneda, J.A. Planell, Enhanced cell-material interactions through the biofunctionalization of polymeric surfaces with engineered peptides, Biomacromolecules. 14 (2013) 2690–2702.

[57]   J. Schindelin, I. Arganda-Carreras, E. Frise, V. Kaynig, M. Longair, T. Pietzsch, S. Preibisch, C. Rueden, S. Saalfeld, B. Schmid, J.Y. Tinevez, D.J. White, V. Hartenstein, K. Eliceiri, P. Tomancak, A. Cardona, Fiji: An open-source platform for biological-image analysis, Nat. Methods. 9 (2012) 676–682.

[58]   P.D.A. Ray, J. Min, R. Tsien, S. Gambhir, Imaging tri-fusion multimodality reporter gene expression in living subjects, Cancer Res. 64 (2004) 1323–1330.

[59]   E. Richtig, G. Langmann, K. Müllner, G. Richtig, J. Smolle, Calculated tumour volume as a prognostic parameter for survival in choroidal melanomas, Eye. 18 (2004) 619–623.

[60]   C.S.M. Pereira, V.M.T.M. Silva, A.E. Rodriguesa, Ethyl lactate as a solvent: Properties,

applications and production processes – a review, Green Chem. 13 (2011) 2658–2671.

[61]   L. Liu, Q. Yu, S. Fu, B. Wang, K. Hu, L. Wang, Y. Hu, Y. Xu, X. Yu, H. Huang, CXCR4 Antagonist AMD3100 Promotes Mesenchymal Stem Cell Mobilization in Rats Preconditioned With the Hypoxia-Mimicking Agent Cobalt Chloride, Stem Cells Dev. 27 (2018) 466–478.

[62]   S.K. Bharti, S. Kakkad, P. Danhier, F. Wildes, M.-F. Penet, B. Krishnamachary, Z.M. Bhujwalla, Hypoxia Patterns in Primary and Metastatic Prostate Cancer Envoronments, Neoplasi. 21 (2019) 239–246.

[63]   S. Zhang, M. Zhou, Z. Ye, Y. Zhou, W.S. Tan, Fabrication of viable and functional pre-vascularized modular bone tissues by coculturing MSCs and HUVECs on microcarriers in spinner flasks, Biotechnol. J. 12 (2017).

[64]   Y. Wang, X. Yuan, K. Yu, H. Meng, Y. Zheng, J. Peng, S. Lu, X. Liu, Y. Xie, K. Qiao, Fabrication of nanofibrous microcarriers mimicking extracellular matrix for functional microtissue formation and cartilage regeneration, Biomaterials. 171 (2018) 118–132.

[65]   X. Wang, Q. Jiao, S. Zhang, Z. Ye, Y. Zhou, W.S. Tan, Perfusion culture-induced template-assisted assembling of cell-laden microcarriers is a promising route for fabricating macrotissues, Biotechnol. J. 9 (2014) 1425–1434.

[66]   M. Chen, M. Zhou, Z. Ye, Y. Zhou, W.S. Tan, Ectopic osteogenesis of macroscopic tissue constructs assembled from human mesenchymal stem cell-laden microcarriers through in vitro perfusion culture, PLoS One. 9 (2014).

[67]   H.A. Declercq, Tamara De Caluwé, O. Krysko, C. Bachert, M.J. Cornelissen, Bone grafts engineered from human adipose-derived stem cells in dynamic 3D-environments, Biomaterials. 34 (2013) 1004–1017.

[68]   V. Brancato, V. Comunanza, G. Imparato, D. Corà, F. Urciuolo, A. Noghero, F. Bussolino, P.A. Netti, Bioengineered tumoral microtissues recapitulate desmoplastic reaction of pancreatic cancer, Acta Biomater. 49 (2017) 152–166.

[69]   L.E. Fitzpatrick, T.C. McDevitt, Cell-derived matrices for tissue engineering and regenerative medicine applications, Biomater. Sci. 3 (2015) 12–24.

[70]   M. Pavel, M. Renna, S.J. Park, F.M. Menzies, T. Ricketts, J. Füllgrabe, A. Ashkenazi, R.A. Frake, A.C. Lombarte, C.F. Bento, K. Franze, D.C. Rubinsztein, Contact inhibition controls cell survival and proliferation via YAP/TAZ-autophagy axis, Nat. Commun. 9 (2018). https://doi.org/10.1038/s41467-018-05388-x.

[71]   T. Kauer, J. Figueiredo, S. Hingtgen, K. Shah, Encapsulated therapeutic stem cells implanted in the tumor resection cavity induce cell death in gliomas, Nat. Neurosci. 15 (2012) 197–204.

[72]   M.J. Resnick, T. Koyama, K.-H. Fan, P.C. Albertsen, M. Goodman, A.S. Matthew, J. Resnick, T.

Koyama, K.-H. Fan, P.C. Albertsen, M. Goodman, Long-Term Functional Outcomes after Treatment for Localized Prostate Cancer, N Engl J Med. 368 (2013) 436–445.

[73]   K. Shah, Mesenchymal Stem Cells engineered for Cancer Therapy, Adv. Drug Deliv. Rev. 64 (2012) 739–748.

[74]   M.L. Kutys, A.D. Doyle, K.M. Yamada, Regulation of cell adhesion and migration by cell-derived matrices, Exp. Cell Res. 139 (2013) 2434–2439.

[75]   L. Marquez-Curtis, A. Janowska-Wieczorek, Enhancing the migration ability of mesenchymal stromal cells by targeting the SDF-1/CXCR4 axis, Biomed. Res. Int. 2013 (2013) 561098.

[76]   X. Jiang, C. Wang, S. Fitch, F. Yang, Targeting tumor hypoxia using nanoparticle-engineered CXCR4- overexpressing adipose-derived stem cells, Theranostics. 8 (2018) 1350–1360.

[77]   E. Hesse, T.E. Hefferan, J.E. Tarara, C. Haasper, R. Meller, C. Krettek, L. Lu, M.J. Yaszemski, Collagen type I hydrogel allows migration, proliferation and osteogenic differentiation of rat bone marrow stromal cells, J Biomed Mater Res A. 94 (2010) 442–449. https://doi.org/10.1161/CIRCULATIONAHA.110.956839.

[78]   L.A. Castagnetta, G. Carruba, Human Prostate Cancer: A Direct Role for Oestrogens, Ciba Found Symp. 191 (1995) 269–286.

[79]   L. Zimmerlin, T. Park, E. Zambidis, V. Donnenberg, A. Donnenberg, Mesenchymal stem cell secretome and regenerative therapy after cancer, Biochimie. 95 (2013) 2235–2245.

[80]   S. Hung, W. Deng, W. Yang, R. Liu, C. Lee, T. Su, R. Lin, D. Yang, C. Chang, W. Chen, H. Wei, J. Gelovani, Mesenchymal stem cell targeting of microscopic tumors and tumor stroma development monitored by noninvasive in vivo positron emission tomography imaging, Clin. Cancer Res. 11 (2005) 7749– 7756.